*J. Fluid Mech.* (1985), *vol.* 156, *pp.* 63–81
*Printed in Great Britain*



# Numerical and asymptotic solutions for merging flow through a channel with an upstream splitter plate

By H. BADR,
Department of Mechanical Engineering, University of Petroleum and Minerals, Dhahran, Saudi Arabia

S. C. R. DENNIS,
Department of Applied Mathematics, University of Western Ontario, London, Ontario N6A 5B9, Canada

S. BATES AND F. T. SMITH
Department of Mathematics, University College, London WC1E 6BT, U.K.

(Received 9 April 1984 and in revised form 29 October 1984)

A numerical and analytical study is described for the divided flow field produced when the flows in two equal parallel channels, separated upstream by an aligned splitter plate, join together to form a single channel beyond the enclosed trailing edge of the plate. On the numerical side the second-order-accurate finite-difference scheme is based on a modified procedure to preserve accuracy and iterative convergence at higher Reynolds numbers $R$. Account is taken also of the influence of the boundedness of the computational domain and of the irregular behaviour of the flow solution at the trailing edge. The numerical solutions are presented for values of $R$ up to 1000. On the analytical side the asymptotic structure of the solution for large $R$ is governed mainly by a long $O(R^{\frac{1}{2}})$ relative lengthscale upstream and beyond the trailing edge. This is followed by a longer $O(R)$ scale far downstream, but effects of practical significance also arise on the nominally tiny scale of $O(R^{-\frac{1}{2}})$. Comparisons between the numerical and the asymptotic results for the wall shear stresses and the wake centreline velocity are made, and overall the agreement seems reasonable. The use of comparisons is believed to strengthen the value of both the numerical and the analytical approaches for these flows.

## 1. Introduction

Branching and merging flows are of especial interest in practical terms in physiological flows and internal machinery dynamics, and they are also of especial interest more generally with regard to the understanding of fundamental fluid dynamics. For such flows can contain some or all of the elements of separation, eddies, reattachment, three-dimensionality, trailing-edge and leading-edge properties, unsteadiness and instability, for instance. Basic to the understanding of these complicated features and their influence, however, is the resolution first of more central and model problems which clarify the nature of a few of the possible main features. That provides the aim of the present work, which is concerned with the steady flow of an incompressible fluid through a divided channel.

The flow involved is of the trailing-edge kind in the sense that it forces two oncoming channel flows to join into one (see below). Many investigations, experimental, numerical and analytical, have been made of the leading-edge kind of branching where one oncoming flow is forced to divide into two, and these are summarized by Smith (1977*a*) and Pedley (1980) among others. Also, external flow past a trailing edge has been the subject of numerous studies. However, the properties of the flow past a trailing edge within a channel have received scant attention as far as we know. The specific geometry of concern here consists of an infinitely long straight channel $|y^*| \leqslant L$, $-\infty < x^* < \infty$ of width $2L$ containing a symmetrically disposed straight splitter plate of semi-infinite extent given by $y^* = 0$, $x^* < 0$. Here $(x^*, y^*)$ are Cartesian coordinates with origin at the trailing edge of the splitter plate, while the corresponding velocity components $(u^*, v^*)$ satisfy $u^* \to 6Q|y^*|(L-|y^*|)L^{-3}$, $v^* \to 0$ far upstream as $x^* \to -\infty$. These conditions reflect the presence of oncoming plane Poiseuille flow in the two channels far upstream, the mass flux in each channel being $Q > 0$. Far downstream the plane Poiseuille flow appropriate to the single wider channel is supposed to emerge, so that $u^* \to 3Q(L^2-y^{*2})/2L^3$, $v^* \to 0$ as $x^* \to \infty$. In between these two limiting flows, the motion is assumed to be steady, laminar and two-dimensional.

The present investigation of this basic merging flow has two main aspects: numerical and analytical. First, calculated solutions of the Navier–Stokes equations are given over a range of values of the Reynolds number $R$ (see §2), up to 1000. The computational method involved here takes account of the discontinuity in the flow solution at the trailing edge, the influence of the finite extent of the computational domain and of its grid spacing and the need for special procedures to maintain accuracy and iterative convergence at larger values of $R$. The method and the results obtained are described in §2. Secondly, the proposed asymptotic properties of the solution for $R \gg 1$ are presented in §3. These are based largely on the viscous–inviscid interactive features that arise on the long $O(R^{\frac{1}{3}}L)$ lengthscale in $x^*$, although other lengthscales also play a significant part. Comparisons between the results of §2 as $R$ increases and the asymptotic predictions of §3 are made in §4. The comparisons concern the wall shear stresses and the centreline velocity of the wake in the region $x^* > 0$, and it is felt that the comparisons add much weight to the value of both the numerical and the analytical approaches used in studying these fluid flows. Further comments are also given in §4.

## 2. Basic equations and numerical treatment

In the usual way we work in terms of dimensionless coordinates $x = x^*/L$, $y = y^*/L$. The corresponding dimensionless velocity components and pressure are defined in terms of dimensional quantities by the equations $u = Lu^*/Q$, $v = Lv^*/Q$, $p = L^2p^*/\rho Q^2$. The density $\rho$ is assumed to be constant, and the Navier–Stokes equations for steady flow are

$$\frac{\partial u}{\partial x} + \frac{\partial v}{\partial y} = 0, \tag{2.1a}$$

$$\left(u\frac{\partial}{\partial x} + v\frac{\partial}{\partial y}\right)(u, v) = -\left(\frac{\partial}{\partial x}, \frac{\partial}{\partial y}\right)p + R^{-1}\nabla^2(u, v), \tag{2.1b}$$

where $R = UL/\nu$ and $U = Q/L$. In the numerical treatment it is convenient to work in terms of the dimensionless stream function $\psi$ and vorticity $\zeta$ defined by the equations

$$\left.\begin{aligned} u = \frac{\partial \psi}{\partial y}, \quad v = -\frac{\partial \psi}{\partial x}; \\ \zeta = \frac{\partial v}{\partial x} - \frac{\partial u}{\partial y}. \end{aligned}\right\} \tag{2.2}$$

Then the Navier–Stokes equations can be expressed as

$$\nabla^2 \psi = -\zeta, \tag{2.3}$$

$$\nabla^2 \zeta = R\left(u \frac{\partial \zeta}{\partial x} + v \frac{\partial \zeta}{\partial y}\right), \tag{2.4}$$

where $\nabla^2 \equiv \partial^2/\partial x^2 + \partial^2/\partial y^2$.

The boundary conditions for the problem are that, in the first place, for $-\infty < x < \infty$,

$$\psi = \begin{cases} 0 & (y = 0), \\ 1 & (y = 1) \end{cases} \tag{2.5a}$$

and

$$\frac{\partial \psi}{\partial y} = 0 \quad (y = 1). \tag{2.5b}$$

Next, for $x > 0$,

$$\zeta = 0 \quad (y = 0) \quad \text{and} \quad \psi \to \tfrac{1}{2} y(3 - y^2) \quad (x \to \infty). \tag{2.5c,d}$$

Finally, for $x < 0$,

$$\frac{\partial \psi}{\partial y} = 0 \quad (y = 0) \quad \text{and} \quad \psi \to y^2(3 - 2y) \quad (x \to -\infty). \tag{2.5e,f}$$

The two equations (2.3) and (2.4) can be solved numerically subject to the set of conditions (2.5) by a finite-difference procedure using a square grid with grid lines parallel to the axes of $x$ and $y$. By virtue of symmetry properties, the solution is required only for $y > 0$. It is natural to make $y = 0$ and $y = 1$ grid lines and also make the origin 0 a grid point. However, the vorticity is infinite at 0, and some special treatment of the situation near this point is required. This special treatment will be described shortly.

Numerical solutions of (2.3) and (2.4) were obtained using the finite-difference approximations proposed by Dennis & Hudson (1978). On the square grid of side $h$ we denote approximations to the functions $\psi$ and $\zeta$ at a typical set of grid points $(x_0, y_0)$, $(x_0 + h, y_0)$, $(x_0, y_0 + h)$, $(x_0 - h, y_0)$ and $(x_0, y_0 - h)$ by means of the respective subscripts 0, 1, 2, 3 and 4. The finite-difference approximation to (2.3) at the point $(x_0, y_0)$ is the usual central-difference formula

$$\psi_1 + \psi_2 + \psi_3 + \psi_4 - 4\psi_0 + h^2 \zeta_0 = 0, \tag{2.6}$$

while for (2.4) Dennis & Hudson give the approximation

$$\begin{aligned} (1 - \tfrac{1}{2}Rhu_0 + \tfrac{1}{8}R^2h^2u_0^2)\,\zeta_1 + (1 - \tfrac{1}{2}Rhv_0 + \tfrac{1}{8}R^2h^2v_0^2)\,\zeta_2 + (1 + \tfrac{1}{2}Rhu_0 + \tfrac{1}{8}R^2h^2u_0^2)\,\zeta_3 \\ + (1 + \tfrac{1}{2}Rhv_0 + \tfrac{1}{8}R^2h^2v_0^2)\,\zeta_4 - \{4 + \tfrac{1}{4}R^2h^2(u_0^2 + v_0^2)\}\,\zeta_0 = 0. \end{aligned} \tag{2.7}$$

This approximation is second-order-accurate, and the associated matrix is diagonally dominant for *all* values of $R$. This greatly improves the convergence properties of the iterative methods of solution which are used, particularly at high Reynolds numbers.

Boundary conditions for $\psi$ are known at all grid points on $y = 0$ and $y = 1$ from (2.5$a$). On $y = 0$, $\zeta$ is given by (2.5$c$) for $x > 0$, and for $x < 0$ it is calculated at all grid points using (2.5$e$). A similar calculation is carried out on $y = 1$ using (2.5$b$). In both cases the formula for calculating $\zeta_B$ at these points on the solid boundaries is based on the method of Woods (1954), and yields

$$\zeta_B = -\frac{3\psi_I}{h^2} - \tfrac{1}{2}\zeta_I, \tag{2.8}$$

where the subscript I denotes a value at the first internal grid point adjacent to the boundary grid point B. The iterative solution of the sets of equations (2.6) and (2.7) subject to the conditions (2.5) and (2.8) follows standard procedures similar to those described by Dennis & Smith (1980), and need not be given in detail.

One grid point that does need special attention is the origin itself at the trailing edge of the plate, where the vorticity is singular. This is dealt with by adapting to the present case a method described by Bramley & Dennis (1982$b$, 1984). A local expansion (see Moffatt 1964) near the origin of the $(x, y)$-coordinates is taken in the form

$$\psi \sim r^\lambda f(\theta), \tag{2.9a}$$

where $(r, \theta)$ are polar coordinates. This expansion is assumed locally to satisfy $\nabla^4\psi = 0$ and, since $\psi$ is an odd function of $\theta$, $f(\theta)$ may be taken in the form

$$f(\theta) = A \sin\lambda\theta + B \sin(\lambda - 2)\theta, \tag{2.9b}$$

where it is easily found that the admissible values of $\lambda$ are the roots of

$$\sin 2(\lambda - 1)\pi = 0;$$

thus

$$\lambda = 1 + \tfrac{1}{2}n, \quad n = 1, 2, \ldots. \tag{2.9c}$$

It is then found that to satisfy the boundary conditions on the plate we must put $A = -B$. The leading term of (2.9$a$) is

$$\psi \sim Ar^{\frac{3}{2}}(\sin\tfrac{1}{2}\theta + \sin\tfrac{3}{2}\theta), \tag{2.10}$$

and the corresponding expression for the vorticity is

$$\zeta \sim 2Ar^{-\frac{1}{2}} \sin\tfrac{1}{2}\theta. \tag{2.11}$$

From (2.10) the stream function is not singular at the origin, and so there is strictly no difficulty in applying the finite-difference equations (2.6) at the point $x = 0, y = h$, which is the only grid point adjacent to the origin where they need be applied. On the other hand, we cannot apply (2.7) at this point, since this would involve a knowledge of $\zeta$ at the origin, which is singular. We therefore proceed in the following way.

The assumption is made that $h$ is small enough for (2.11) to give a satisfactory approximation near 0. We then determine the constant $A$ by satisfying (2.11) at the point $x = -h$, $y = 0$, which is a point where $\zeta$ is determined using (2.8). From the approximation to $\zeta$ so determined, we can calculate $\zeta(0, h)$ using (2.11). The required formula is

$$\zeta(0, h) = \zeta(-h, 0)/\sqrt{2}. \tag{2.12}$$

A very similar procedure was used by Smith & Dennis (1981) and Bramley & Dennis (1982$a$, 1984). It was carefully checked by alternative means and found to be quite accurate. In the present work the formula (2.12) is incorporated into the iterative

procedure of solution as follows. Following an iterative sweep of all internal grid points (including $(0, h)$) for $\psi$ using (2.6), a similar sweep of all points except $(0, h)$ is made using (2.7) for $\zeta$. Then boundary values are calculated using (2.8), and finally (2.12) is applied. This iteration is then repeated. It is necessary to use a relaxation factor in applying (2.8); this is easily found by trial for a given value of $R$. Generally speaking, this factor has to be decreased as $R$ is increased.

Numerical solutions were obtained for the four grid sizes $h = \frac{1}{20}, \frac{1}{40}, \frac{1}{80}$ and $\frac{1}{160}$ for each of the Reynolds numbers $R = 1$, 10, 100, 500 and 1000. It is necessary in the present formulation to limit the boundaries both upstream and downstream to boundaries at finite distances from the origin on which it is reasonable to assume that the respective conditions (2.5*f*) and (2.5*d*) of Poiseuille flow are satisfied approximately. Bramley & Dennis (1982*a*, *b*) have indicated that it is relatively easy to do this upstream, but more difficult downstream, as might be expected. However, the present problem is rather similar in the aspect of upstream and downstream boundary conditions to that considered by Dennis & Smith (1980). The discussions given there are quite appropriate in the present case and the imposition of the conditions (2.5*d*,*f*) at relatively small distances of two or three times the smaller channel width both upstream and downstream of the trailing edge generally were found to be satisfactory. Checks were made by moving the positions of these boundaries. The results presented here are believed to be accurate, based on the evidence of these tests.

We first present results for the local dimensionless coefficient of skin friction $c_f$ on the plate. This is determined from the shear stress $\tau(x) = \mu(\partial u^*/\partial y^*)\,[y^* = 0]$ for $x < 0$ by the definition

$$c_f = \frac{\tau}{\frac{1}{2}\rho U^2} = -\frac{2\zeta(x, 0)}{R}. \tag{2.13}$$

We can calculate this coefficient everywhere when $x < 0$, except at the trailing edge $x = 0$, where it is singular. However, the expression (2.11) indicates that as $x \to 0-$

$$c_f \sim a(R)\,(-x)^{\frac{1}{2}}, \tag{2.14}$$

so that if we determine $a(R)$ the variation of the skin friction near enough to $x = 0$ is known.

Table 1 gives estimates of $a(R)$ from the four grid sizes for each value of $R$. These values have been obtained by calculating $a(R)$ to satisfy (2.14) using the value of $c_f$ at the nearest grid point to $x = 0$ (i.e. $x = -h$). Naturally, as $h \to 0$ we might expect to get better estimates of $a(R)$ by this process for two reasons. First, the point at which the determination is made will be nearer to $x = 0$, and thus (2.14) should be a more adequate approximation; secondly, the value of $c_f$ should itself be more accurate, having been calculated from a solution on a finer grid. If we assume that an approximation $\alpha_h(R)$ to $a(R)$ is obtained with a given grid $h$ and that, by use of central differences, we can assume the expansion

$$\alpha_h(R) = a(R) + b(R)\,h^2 + c(R)\,h^4 + \ldots \tag{2.15}$$

in even powers of $h$, we may attempt to estimate $a(R)$ by the process of $h^2$ extrapolation. This procedure was found to yield very satisfactory estimates of the length of upstream vortices in the case of flow in a channel with a step considered by Dennis & Smith (1980); similar results might be expected for $a(R)$ in the present case. The final values of $a(R)$ for each $R$ obtained by repeated $h^2$ extrapolation from the values calculated using the four separate grids are given in the last row of table 1. Although it is probable that the theoretical variation of $a(R)$ with $R$ is of the form

| $h \backslash R$ | 1 | 10 | 100 | 500 | 1000 |
|---|---|---|---|---|---|
| $\frac{1}{20}$ | 5.093 | 1.398 | 0.3795 | 0.1680 | 0.1195 |
| $\frac{1}{40}$ | 4.965 | 1.302 | 0.3126 | 0.1273 | 0.0904 |
| $\frac{1}{80}$ | 4.891 | 1.249 | 0.2737 | 0.1023 | 0.0699 |
| $\frac{1}{160}$ | 4.850 | 1.223 | 0.2528 | 0.0875 | 0.0577 |
| $E$ | 4.834 | 1.212 | 0.2446 | 0.0816 | 0.0529 |

TABLE 1. Values of $R^{\frac{1}{2}}\alpha_h(R)$ estimated from various grid sizes at values of $R$ in the range $R = 1$ to $R = 1000$. The value $E$ is the final estimate of $R^{\frac{1}{2}}a(R)$ obtained by repeated $h^2$ extrapolation from the four values on various grids. See (2.14), and also figure 6(*b*).

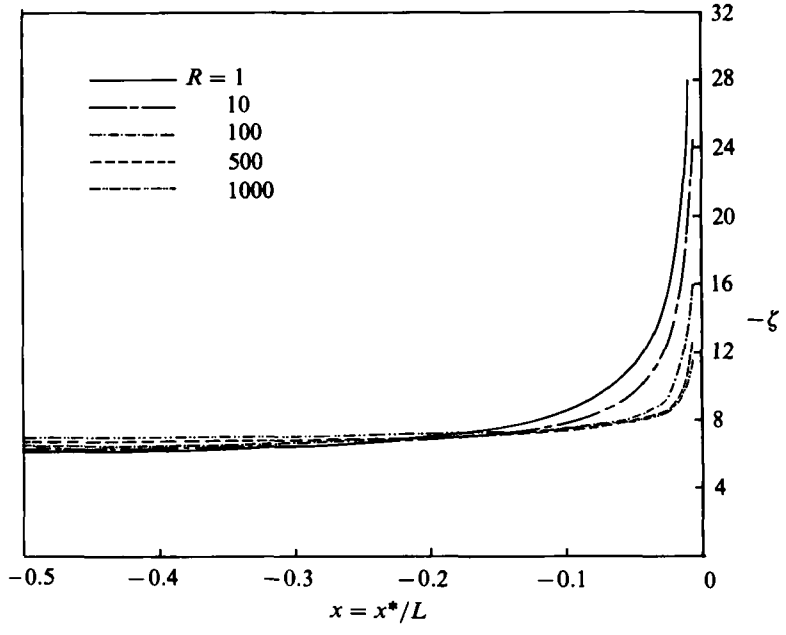


FIGURE 1. Variation of vorticity $\zeta$ on the splitter plate in $x < 0$, for various values of $R$, obtained computationally as described in §2.

$a(R) \sim bR^{-p}$ $(p > 0)$ when $R$ is large, it is not possible to deduce any information regarding such a variation from the final values in table 1 (see also §§3, 4).

In figure 1 the distribution of vorticity over the plate is given for the Reynolds numbers considered. In order to be consistent with the results for $c_f$ in the final row of table 1, the curves in figure 1 have been obtained using a similar procedure of repeated $h^2$ extrapolations. We may note, however, that the final results presented are scarcely distinguishable graphically from the results of the calculations using the finest grid, $h = \frac{1}{160}$. In figure 2 the velocity on the centreline of the downstream channel is shown. The main effect here is that, as the Reynolds number increases, the distance downstream of the trailing edge at which the Poiseuille velocity distribution is recovered increases. In fact, only for the lowest of the Reynolds numbers $R = 1$ and 10 is the Poiseuille flow attained, approximately, within the range $x \leqslant 2$ shown in figure 2. For higher values of $R$ the recovery length is much longer, and it is not possible to say what it is with any reasonable certainty.

The point here is that, as explained by Dennis & Smith (1980), when the Poiseuille flow downstream is applied as a boundary condition it does not give a very good *local*

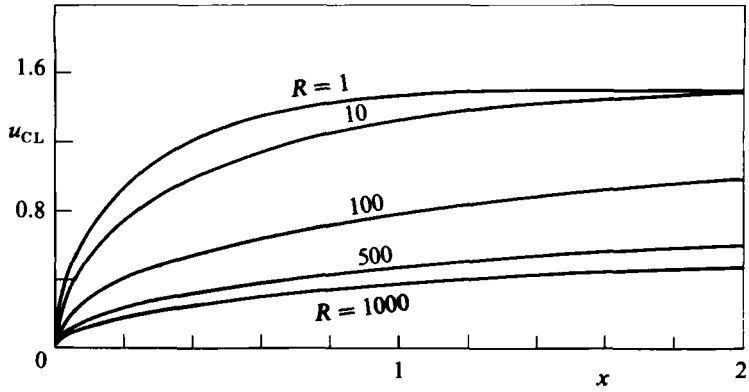


FIGURE 2. The calculated development of the velocity $u_{CL}$ at the channel centreline $y = 0$ for $x > 0$, downstream of the trailing edge, at various $R$-values, from §2.

approximation to the flow. Moreover, Bramley & Dennis (1982*a*) found that it was not possible to construct a satisfactory method of approximation to the flow downstream using its eigenfunction expansion corresponding to the linearized equation giving the first-order perturbation from the Poiseuille flow, although it was possible to derive a satisfactory method of approximation to the upstream flow. However, when Poiseuille flow is assumed downstream at a given station, it is found by trial that the effect of making this rather crude approximation at a finite but reasonably large distance from the trailing edge does not seriously affect the flow at large enough distances upstream from the station of the applied boundary condition. In other words, the effect of the imposition of Poiseuille flow downstream as a boundary condition does not spread back very far into the upstream flow. Thus it is possible to test a solution by applying the Poiseuille-flow condition at several stations downstream, and finding by trial an upstream region in which the flow does not change appreciably when the station of application of the downstream boundary condition is altered. Such a procedure has been used in the present computations. The computed solutions are accurate up to a reasonable distance from the trailing edge, but of course it cannot be said what further distance would be necessary for the flow to approach the actual Poiseuille velocity profile. In the eigenfunction expansion given by Bramley & Dennis (1982*a*) the eigenvalues are not well separated for high Reynolds number, and many terms would be needed to describe the downstream flow. Nevertheless, over the range shown in figure 2 the results are accurate, graphically at least, even for the higher values of $R$.

A similar situation exists in figures 3(*a–e*), which show the variation of the dimensionless vorticity on the upper wall for the five cases $R = 1$, 10, 100, 500 and 1000. As $R$ increases, the decay of vorticity to its downstream value takes place over an increasingly longer scale of $x$. However, despite the necessity of imposing the vorticity distribution of Poiseuille flow at a finite distance downstream, the effect on the vorticity distribution does not spread greatly upstream, and generally the results shown in the figures are accurate over the range shown. Perhaps at the highest Reynolds number there still remains some grid dependence, even at the smallest value $h = \frac{1}{160}$, but even here we believe the results to be substantially correct, especially the extrapolated values in table 1.

It might have been desirable to adopt a coordinate transformation to deal with the downstream flow, because of the increasing lengthscale in $x$ downstream as $R$ increases. Such a device was used by Bramley & Dennis (1982*b*, 1984) in calculating

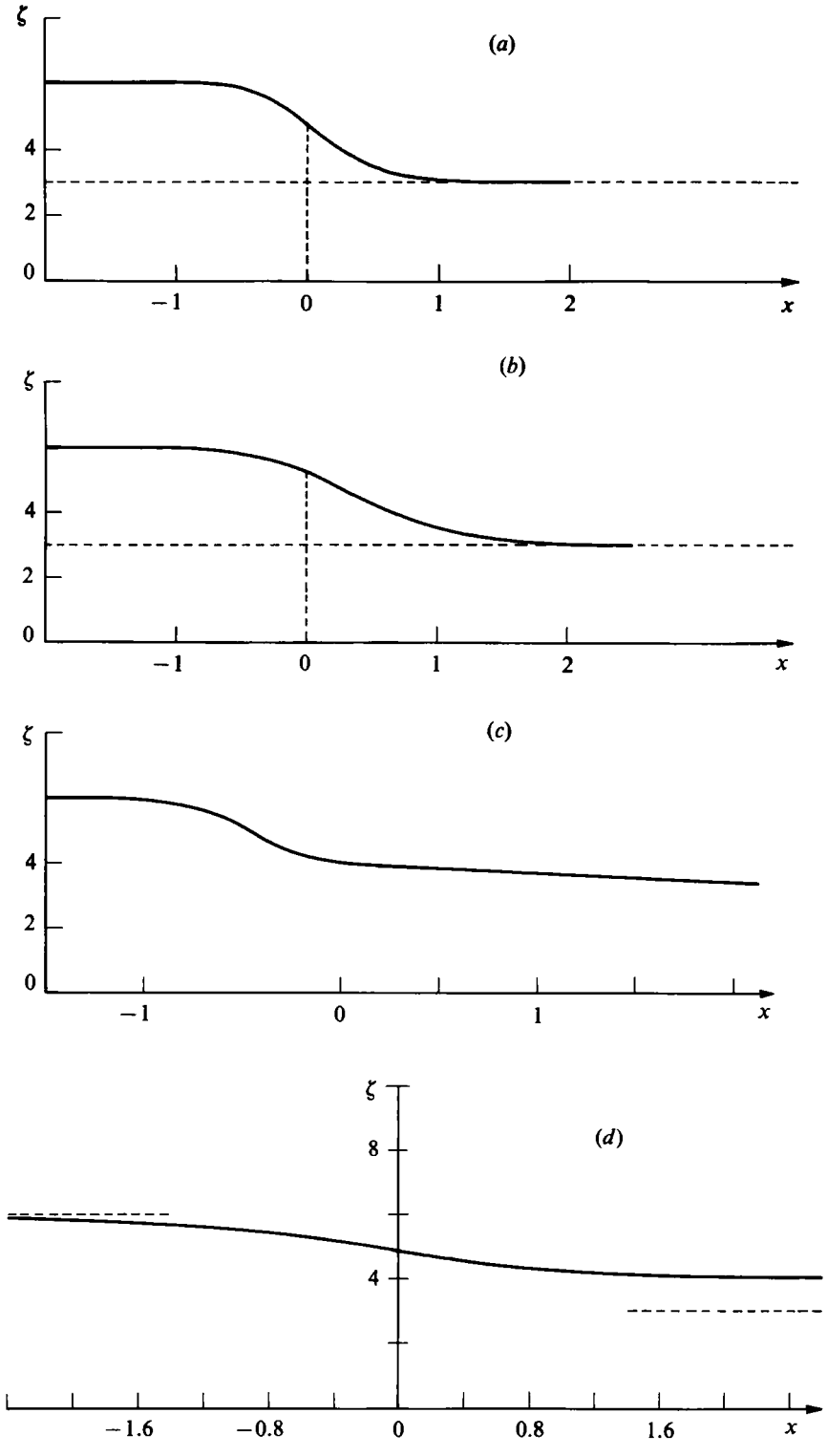


FIGURE 3 (*a–d*). For caption see opposite page.

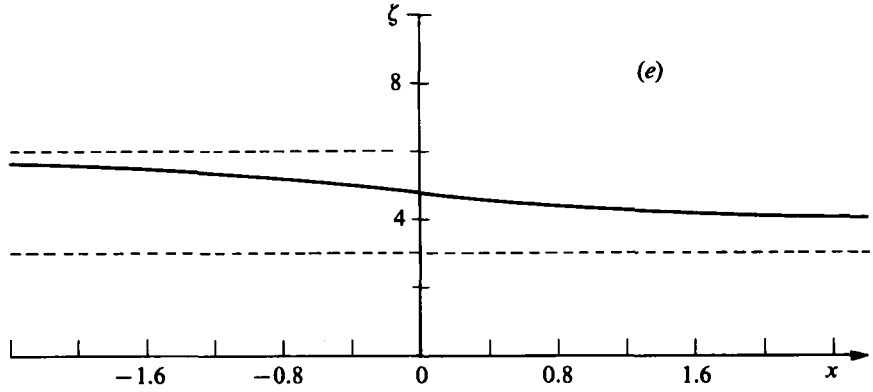


FIGURE 3. The vorticity distributions $\zeta(x, 1)$ on the upper wall, versus $x$: for (*a*) $R = 1$; (*b*) 10; (*c*) 100; (*d*) 500; (*e*) 1000.

flow in a branched channel, where a logarithmic transformation was employed in a region downstream of the point of branching. The present calculations, however, were carried out prior to the work of Bramley & Dennis and before the idea of employing such a transformation was conceived. The number of iterative loops through the sets of equations (2.6)–(2.8) to achieve a solution was many thousands in some cases, particularly for the higher values of $R$. The main reason for this is the particularly sensitive nature of the calculation of boundary values of vorticity using (2.8). It has been explained that a relaxation factor must be employed in using (2.8) and that this may be decreased as $R$ is increased. This leads to a great increase in the number of iterations, and any attempt to accelerate the procedure makes the calculation (2.8) unstable. The main calculations were carried out partly on the CYBER 73 and partly on the PRIME 400 compilers at the University of Western Ontario. Because of this division it is not feasible to give a reasonable estimate of the computer time used in each calculation, although recent recalculations with $h = \frac{1}{20}$ took between 1 min (for $R = 1$) and 32 min (for $R = 1000$) on an Amdahl 580.

## 3. Asymptotic theory for large $R$

The theory for $R \gg 1$ is based on the free-interaction structure of Smith (1977*b*), for we propose that the long axial lengthscale $x = O(R^{\frac{1}{7}})$, surrounding the trailing edge at $x = 0$, governs the major effects of the trailing edge. On that scale $x = R^{\frac{1}{7}}X$ say, with $X = O(1)$, and the solution of (2.1)–(2.5) subdivides into three distinct regions I–III (see figure 4*a*).

In region I, which is the slightly perturbed core of the channel flow, $0 < y < 1$ and

$$(u, v, p) = (U_0(y), 0, 0) + (R^{-\frac{1}{7}}u_1, R^{-\frac{3}{7}}v_1, R^{-\frac{4}{7}}p_1) + \ldots, \tag{3.1}$$

where $U_0(y) \equiv 6(y - y^2)$. From substitution into (2.1*a*, *b*) we find the perturbation solutions

$$\left.\begin{aligned} u_1(X, y) = A(X)\, U_0'(y), \quad v_1(X, y) = -A'(X)\, U_0(y), \\ p_1(X, y) = P(X) + A''(X) \int_0^y U_0^2(y_1)\, \mathrm{d}y_1 \end{aligned}\right\} \tag{3.2}$$

where $P$, the pressure along $y = 0$, and $A$, the negative displacement of the core, are unknown functions of $X$. The pressure variation across the core in (3.2) is the vital factor on this lengthscale, and occurs because of the slight curving of the core flow during the negotiation of the trailing edge.

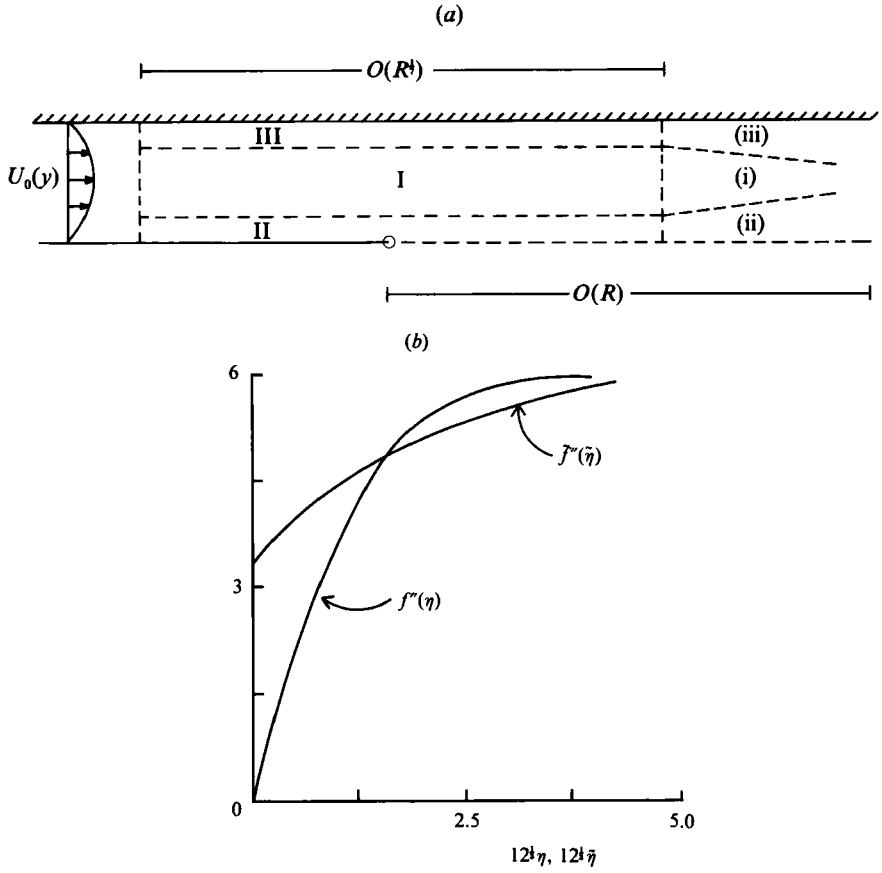


FIGURE 4. (*a*) Schematic diagram, not to scale, of the asymptotic flow structure (I–III) for $R \gg 1$ on the $O(R^{\frac{1}{4}})$ streamwise lengthscale, the continuation into the Goldstein near-wake form ((i)–(iii)) downstream and the Navier–Stokes zone (○) very close to the trailing edge, considered in §3. (*b*) The solution curves for the effective shear stresses $f''$ and $\tilde{f}''$ versus $\eta$ and $\tilde{\eta}$ in the near-wake form governed by (3.22)–(3.27) when $R \gg 1$.

In region II the nonlinear viscous wall layer near $y = 0$, $y = R^{-\frac{3}{7}}Y$ with $Y = O(1)$, and from (3.1) and (3.2)

$$(u, v, p) = (R^{-\frac{3}{7}}U, R^{-\frac{5}{7}}V, R^{-\frac{4}{7}}P(X)) + \ldots. \tag{3.3}$$

The fact that $\partial P/\partial Y = 0$ in (3.3) follows from the transverse momentum equation, while the continuity and axial momentum equations give the classical boundary-layer equations

$$\frac{\partial U}{\partial X} + \frac{\partial V}{\partial Y} = 0, \quad U\frac{\partial U}{\partial X} + V\frac{\partial U}{\partial Y} = -P'(X) + \frac{\partial^2 U}{\partial Y^2}. \tag{3.4}$$

The boundary conditions on (3.4) are

$$\left.\begin{aligned} U = V = 0 \quad (X < 0), \\ \frac{\partial U}{\partial Y} = V = 0 \quad (X > 0) \end{aligned}\right\} \quad (Y = 0), \tag{3.5}$$

$$(U, V, P, A) \to (6Y, 0, 0, 0) \quad (X \to -\infty), \tag{3.6}$$

$$U \sim 6(Y + A(X)) \quad (Y \to \infty). \tag{3.7}$$

Here (3.5) reflects the presence of the trailing edge at $X = 0$, while (3.6) and (3.7) respectively match the flow with the oncoming Poiseuille form (2.5$f$) far upstream and with the core motion.

Similarly, in region III, the nonlinear viscous layer near the wall at $y = 1$, we have $y = 1 - R^{-\frac{3}{7}}\tilde{Y}$, with $\tilde{Y} = O(1)$, and

$$(u, v, p) = (R^{-\frac{2}{7}}\tilde{U}, -R^{-\frac{5}{7}}\tilde{V}, R^{-\frac{4}{7}}\tilde{P}(X)) + \ldots. \tag{3.8}$$

Hence, from (2.1)–(2.5), the controlling equations and boundary conditions are

$$\frac{\partial \tilde{U}}{\partial X} + \frac{\partial \tilde{V}}{\partial \tilde{Y}} = 0, \quad \tilde{U}\frac{\partial \tilde{U}}{\partial X} + \tilde{V}\frac{\partial \tilde{U}}{\partial \tilde{Y}} = -\tilde{P}'(X) + \frac{\partial^2 \tilde{U}}{\partial \tilde{Y}^2}, \tag{3.9}$$

$$\tilde{U} = \tilde{V} = 0 \quad (\tilde{Y} = 0, \text{ all } X), \tag{3.10}$$

$$(\tilde{U}, \tilde{V}, \tilde{P}) \to (6\tilde{Y}, 0, 0) \quad (X \to -\infty), \tag{3.11}$$

$$\tilde{U} \sim 6(\tilde{Y} - \tilde{A}(X)) \quad (Y \to \infty). \tag{3.12}$$

The conditions (3.11) and (3.12) are analogous to (3.6) and (3.7), while (3.10) is the no-slip condition of (2.5$a, b$).

Two more conditions are necessary, to define fully the trailing-edge problem on this lengthscale, and these are

$$\tilde{P}(X) - P(X) = \tfrac{6}{5}A''(X), \tag{3.13}$$

$$\frac{\mathrm{d}P}{\mathrm{d}X}, \frac{\mathrm{d}\tilde{P}}{\mathrm{d}X} \to 0 \quad \text{as } X \to \infty, \tag{3.14}$$

upon which comments will be made in the next paragraph. The task set, then, is the numerical one of solving the two linked nonlinear wall-layer problems (3.4)–(3.7) and (3.9)–(3.12) together with the pressure–displacement relation (3.13) and the downstream condition (3.14). The flow response far upstream of the trailing edge, on this $O(R^{\frac{1}{7}})$ lengthscale, starts in the exponential eigensolution form

$$\tilde{P}(X) \approx \tilde{P}_{-\infty}\, \mathrm{e}^{\kappa X} \quad (X \to -\infty), \tag{3.15}$$

where $12^{\frac{1}{7}}\kappa = 5.731$ (Smith 1977), but the constant $\tilde{P}_{-\infty}$ remains unknown in advance. Indeed, the numerical task in essence is to find the value of $\tilde{P}_{-\infty}$ in (3.15) such that (3.14) is satisfied downstream (cf., in related interaction problems, Stewartson 1970; Smith & Stewartson 1973; Daniels 1974; Smith 1978).

Before the solution of (3.4)–(3.7) and (3.9)–(3.14) is described, some explanation of the constraints (3.13) and (3.14) is called for. Clearly (3.13) follows from the matching of the pressures between the core and wall layer III by use of (3.2). However, condition (3.14) must be imposed to ensure a match as $X \to \infty$ with the following wake flow that ensues on the longer axial lengthscale $O(R)$ beyond the trailing edge. On the latter scale, where $x = R\overline{X}$, with $\overline{X} > 0$ and $O(1)$, $u$ and $p$ are $O(1)$ and $v$ is $O(R^{-1})$, so that the governing equations throughout the half-channel $0 \leqslant y \leqslant 1$ are then the boundary-layer equations (Wilson 1971; Van Dyke 1970; Smith 1976)

$$\frac{\partial u}{\partial \overline{X}} + \frac{\partial \overline{V}}{\partial y} = 0, \quad u\frac{\partial u}{\partial \overline{X}} + \overline{V}\frac{\partial u}{\partial y} = -p'(\overline{X}) + \frac{\partial^2 u}{\partial y^2} \tag{3.16}$$

from (2.1$a, b$) to leading order. Here $v = R^{-1}\overline{V}$, and the balance of transverse

momentum requires that $\partial p/\partial y = o(1)$ when $\bar{X} > 0$ is $O(1)$. The boundary conditions on (3.16) are

$$\left.\begin{aligned} u = \bar{V} = 0 \quad (y = 1), \\ \frac{\partial u}{\partial y} = \bar{V} = 0 \quad (y = 0) \end{aligned}\right\} \quad (X > 0) \tag{3.17, 3.18}$$

from (2.5*a*–*c*). The starting condition on (3.16) is similar to that imposed in more standard near-wake analyses (Goldstein 1930), namely

$$u \to U_0(y) \quad (\bar{X} \to 0+,\ 0 < y < 1). \tag{3.19}$$

For on this $O(R)$ axial lengthscale the nonlinear disturbances produced on the smaller $O(R^{\frac{1}{3}})$ lengthscale above are negligible, allowing a direct match with the Poiseuille flow of (2.2*a*) except along $y = 0, 1$, where the trailing-edge conditions and the effects of layers II and III above must be recognized. The solution, necessarily numerical, of (3.16)–(3.19) would describe most of the development from the oncoming Poiseuille flow (2.5*f*) to the eventual Poiseuille flow (2.5*d*) attained as $\bar{X} \to \infty$, but what is more important to us at present is the near-wake form of the solution of (3.16)–(3.18) as $\bar{X} \to 0+$. A consistent (and, we believe, the only consistent) such form is based on the expansion

$$p \approx P_1 \bar{X}^{\frac{2}{3}} + O(\bar{X}) \quad (\bar{X} \to 0+) \tag{3.20}$$

of $p(\bar{X})$, where $P_1$ is a constant to be determined. With (3.20) the solution of (3.16)–(3.19) splits into three zones (i)–(iii) as $\bar{X} \to 0+$ (figure 4*a*). In (i), where $0 < y < 1$,

$$u = U_0(y) + A_1 \bar{X}^{\frac{1}{3}} U_0'(y) + O(\bar{X}^{\frac{2}{3}}), \tag{3.21}$$

where the constant $A_1$ is unknown. In (ii), where $y = O(\bar{X}^{\frac{1}{3}})$ and $\eta = y\bar{X}^{-\frac{1}{3}}$,

$$u = \bar{X}^{\frac{1}{3}} f'(\eta) + O(\bar{X}^{\frac{2}{3}}),$$

and $f(\eta)$ satisfies the nonlinear ordinary differential equation and boundary conditions

$$f''' + \tfrac{2}{3} f f'' - \tfrac{1}{3} f'^2 = \tfrac{2}{3} P_1 \quad \text{(from (3.16))}, \tag{3.22}$$

$$f(0) = f''(0) = 0 \quad \text{(from (3.18))}, \tag{3.23}$$

$$f' \sim 6(\eta + A_1) \quad (\eta \to \infty). \tag{3.24}$$

Here (3.24) follows from matching (ii) with (i). Similarly, in (iii), where $y - 1 = O(\bar{X}^{\frac{1}{3}})$ and $\tilde{\eta} = (1-y)\bar{X}^{-\frac{1}{3}}$, $u = \bar{X}^{\frac{1}{3}} \tilde{f}'(\tilde{\eta}) + O(\bar{X}^{\frac{2}{3}})$ and so

$$\tilde{f}''' + \tfrac{2}{3} \tilde{f} \tilde{f}'' - \tfrac{1}{3} \tilde{f}'^2 = \tfrac{2}{3} P_1 \quad \text{(from (3.16))}, \tag{3.25}$$

$$\tilde{f}(0) = \tilde{f}'(0) = 0 \quad \text{(from (3.17))}, \tag{3.26}$$

$$\tilde{f}' \sim 6(\tilde{\eta} - A_1) \quad (\tilde{\eta} \to \infty). \tag{3.27}$$

The solution of the interlinked similarity problems (3.22)–(3.24) and (3.25)–(3.27) was obtained numerically by adapting the numerical procedure to be described below, is shown in figure 4(*b*) and has the properties

$$\tfrac{2}{3} P_1 = 0.085 \times 12^{\frac{4}{3}}, \quad \tfrac{1}{2} A_1 = 0.340 \times 12^{-\frac{1}{3}}, \quad \tilde{f}''(0) = 3.281. \tag{3.28}$$

We note that a check on the numerical accuracy here was made by recalculating the solution of Goldstein's (1930) near-wake problem, and the difference between our

solution and Goldstein's was found to be only 1 in the fourth significant figure. Also the matching of the near-wake form in (3.20)–(3.28) as $\bar{X}\to 0+$ with the previous $O(R^{\frac{1}{8}})$ structure of (3.1), (3.3) and (3.8) as $X\to\infty$ there verifies the imposition of the constraint (3.14), from (3.20) and (3.3). Indeed the results (3.28) with (3.20) and (3.21) lead us to expect the asymptotes

$$P(X)\sim\tilde{P}(X)\sim 0.128(144X)^{\frac{6}{5}},\quad A(X)\sim 0.680(\tfrac{1}{12}X)^{\frac{1}{5}}\quad(X\to\infty) \tag{3.29}$$

in view of (3.1)–(3.3), (3.8) and (3.13).

The solution of (3.4)–(3.7) and (3.9)–(3.14) was sought by modifying the program of Smith (1977), in which paper most details of the central-difference numerical scheme used may be found. A shooting technique was employed to find the solution of (3.4)–(3.7) and (3.9)–(3.13) satisfying (3.14). Thus a number of guesses were made for the value $b=\tilde{P}(X_{-\infty})$ of $\tilde{P}$ at a suitably large negative value $X_{-\infty}$ of $X$; for each the free-interaction solution was then allowed to develop up to the trailing edge at $X=0$, and the wake conditions in (3.5) were imposed at stations beyond $X=0$. Such guesses always led to divergence from the required downstream condition (3.14) (cf. Stewartson 1970; Smith & Stewartson 1973; Daniels 1974; Smith 1978), but only two kinds of such divergence are possible (figure 5*a*), and the required solution satisfying (3.14) lies between them. In practice the criterion on $\tilde{\tau}\equiv\partial\tilde{U}/\partial\tilde{Y}(X,0)$,

$$\tilde{\tau}(X)\to 3.281\quad(X\to\infty) \tag{3.30}$$

(from (3.28)), proved easier to seek in the refinement of the value of $b$ than did (3.14). The refinement leads to the solution of (3.4)–(3.7) and (3.9)–(3.14) shown in figure 5(*b*). We found the properties

$$\tilde{\tau}(0)=4.91,\quad \tau(0-)=7.22,\quad \frac{P(0)}{12^{\frac{10}{7}}}=-0.0186,\quad \frac{\tilde{P}(0)}{12^{\frac{10}{7}}}=0.0164 \tag{3.31}$$

using a grid of height (in $\hat{Y}=12^{\frac{3}{7}}Y$) $\hat{Y}_{\infty}=10$, with step lengths

$$\Delta\hat{Y}=0.025\quad\text{in }\hat{Y},\quad \Delta\hat{X}=0.01\quad\text{in }\hat{X}=(12)^{-\frac{1}{7}}X$$

and with $\hat{X}_{-\infty}=12^{-\frac{1}{7}}X_{-\infty}=-0.86$. Here $\tau\equiv\partial U/\partial Y(X,0)=0$ for $X>0$, while the factors involving powers of 12 here and elsewhere allow for the different non-dimensionalization of Smith (1977*b*). As checks on the accuracy we found the respective values 4.93, 7.20, −0.0181 and 0.0160 instead of those in (3.31) when the grid size was doubled to $\Delta\hat{Y}=0.05$, $\Delta\hat{X}=0.02$, and the respective values 4.99, 7.13, −0.0171 and 0.0151 when the grid size was quadrupled to $\Delta\hat{Y}=0.10$, $\Delta\hat{X}=0.04$, keeping $\hat{Y}_{\infty}$ fixed at 10. When the grid height was doubled to $\hat{Y}_{\infty}=20$ with $\Delta\hat{Y}=0.10$, $\Delta\hat{X}=0.04$ the four respective values last referred to were reproduced identically, and the same proved true when $\hat{X}_{-\infty}$ was set equal to −0.70. Accordingly $(\Delta\hat{X})^2+(\Delta\hat{Y})^2$ extrapolation works well, and we believe the numerical values for $\tau(0-)$ and $\tilde{\tau}(0)$ in (3.31) to be accurate to within 0.2% or less.

The asymptotic forms for $P$, $\tilde{P}$, $A$ and $\tilde{\tau}$ in (3.29) and (3.30), shown in figure 5(*b*), provide a further overall check on our numerical solution. Also shown in figure 5(*b*) is the local form of the pressure $P$ just beyond the trailing edge on the present $O(R^{\frac{1}{8}})$ lengthscale. The latter form is

$$P(X)\sim P(0-)+0.6133(\tau(0-))^{\frac{4}{5}}X^{\frac{2}{5}}\quad(X\to 0+), \tag{3.32}$$

and follows from a local analysis for $0<X\ll 1$ of the solution to (3.4)–(3.7) and (3.9)–(3.14) similar to that of (3.20)–(3.28) further downstream. In the local analysis both of the wall layers II and III develop double structures as $X\to 0+$. Within the

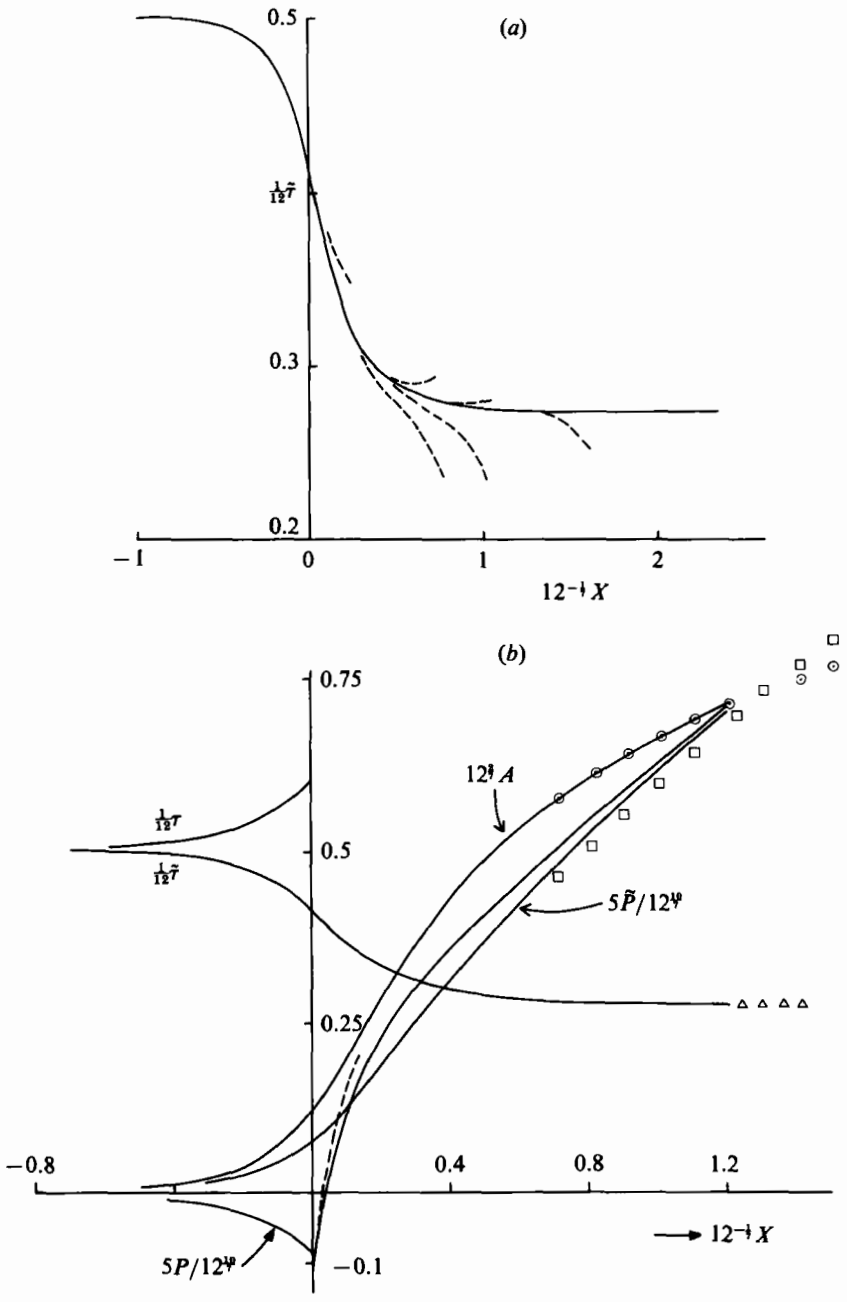


FIGURE 5. (*a*) Samples of the trial numerical solutions (– – –, satisfying (3.4)–(3.7) and (3.9)–(3.13)) used in the interpolation for the full solution (——, satisfying (3.4)–(3.7), (3.9)–(3.13) and (3.30)) for the skin friction $\tilde{\tau}$ versus $X$. (*b*) The solution of (3.4)–(3.7) and (3.9)–(3.14) for $\tau$, $\tilde{\tau}$, $P$, $\tilde{P}$ and $A$ versus $X$ on the $O(R^{\frac{1}{4}})$ lengthscale in $x$ when $R \gg 1$. Also shown for comparison purposes are the downstream ($X \to \infty$) asymptotes ○ ○ ○, □ □ □ and △ △ △ for $A$ in (3.29), $P$ and $\tilde{P}$ in (3.29), and $\tilde{\tau}$ in (3.30) respectively, and the asymptote – – – locally ($X \to 0+$) for $P$ from (3.32). The solution for the reduced centreline velocity $U(X, 0)$ versus $X$ in $X > 0$ is given in figure 6(*c*) as the limit curve for $R^{\frac{1}{4}}u_{\mathrm{CL}}\,12^{-\frac{1}{4}}$ versus $(12R)^{-\frac{1}{4}}x$.

double structure of layer II, $U = X^{\frac{1}{3}}F'(\eta)$ when $\eta = YX^{-\frac{1}{3}}$ is of $O(1)$ and $F(\eta)$ satisfies (3.22)–(3.24) again, with $F$ replacing $f$ and unknown constants $p_1$, $a_1$ replacing $P_1$, $A_1$ respectively there. However, the condition $a_1 = 0$ is necessary: otherwise the implied property $A'(X) \sim \frac{1}{3}a_1 X^{-\frac{2}{3}}$ as $X \to 0+$ would lead to inconsistencies within the double structure of layer III because of the relation (3.13). Hence the solution for $F(\eta)$ and for $p_1$ is that of Hakkinen & Rott (1965), leading to the result (3.32) wherein $p_1$ is the coefficient of $X^{\frac{2}{3}}$. The double structure of layer III is a relatively passive affair, on the other hand, since we find that $\tilde{P}$, $\tilde{P}'$ and $\tilde{P}''$ are continuous at $X = 0$, $\tilde{P}'''$ is finite but discontinuous as $X \to 0\pm$, and $A$ has only a mild $o(X^{\frac{2}{3}})$ irregularity, of the form

$$A(X) \sim A(0-) + XA'(0-) + \tfrac{1}{2}X^2A''(0-) - \tfrac{3}{16}p_1 X^{\frac{8}{3}} \tag{3.33}$$

as $X \to 0+$. The agreement between the full solution and the asymptotes of (3.29), (3.30) and (3.32) (see figure 5*b*) and (3.33) is an encouraging feature.

Comparisons between the present, large-$R$, theory and the calculations for finite values of $R$ are given below. We note in advance the existence of a small passive Navier–Stokes zone of non-uniformity in the above theory on a lengthscale $x, y = O(R^{-\frac{1}{2}})$ near the trailing edge where the discontinuities in $\tau$ and $P'$ for instance are adjusted (cf. Dijkstra 1974). In fact the solution within this $O(R^{-\frac{1}{2}})$ Navier–Stokes zone is exactly that of Dijkstra (1974) when suitable numerical factors are extracted to account for the values of the pressure $P$ and the skin friction $\tau$ in (3.31) and (3.32) as $X \to 0\pm$ and $R^{\frac{1}{2}}x \to \pm\infty$, and from his calculation we have the prediction

$$\frac{\partial u}{\partial y}(x, 0) \sim [0.800(\tau(0-))^{\frac{3}{4}}R^{-\frac{1}{4}}]\,|x|^{-\frac{1}{2}} \quad (R^{\frac{1}{2}}x \to 0-) \tag{3.34}$$

in particular. Again, this is compared below with the calculations for finite values of $R$.

Some work in this section forms part of Bates' (1978) thesis; he also considers wedge-like junctions, and curvings, of channel flows, by means of the same free-interaction theory, as well as certain other problems of bifurcations, blockages or thermal effects in channel or axisymmetric pipe flows.

## 4. Comparisons and comments

In qualitative terms there is little or no doubt that the numerical solutions of the Navier–Stokes equations (figures 1–3) and the asymptotic predictions (figures 4 and 5) are in general agreement on the most important features of the flow at moderate-to-large Reynolds numbers $R$. The overriding effect of the channel junction here is to produce an increasing slip velocity $u_{\mathrm{CL}}$ beyond the trailing edge. This acceleration draws fluid broadly towards the wake centreline, thus increasing the shear stress $\zeta_{\mathrm{w}}^-$ on the splitter plate, but decreasing the shear stress $\zeta_{\mathrm{w}}^+$ on the outer wall, before the approach to the ultimate plane Poiseuille flow takes place quite far downstream. The effect of the increasing slip velocity is eventually overwhelmed, incidentally, if the two straight channels upstream are made gradually to converge at a significant angle (see Bates 1978; and Smith & Duck 1980). Further qualitative agreement between the results derived from §§2 and 3 is evident in figures 1 and 3, where the increase of upstream influence in the calculated solutions for $\zeta_{\mathrm{w}}^{\pm}$ as $R$ increases is in keeping with the $O(R^{\frac{1}{7}})$ upstream trend proposed in §3 for $R \gg 1$. We turn to quantitative comparisons next. In making these comparisons we believe it important to emphasize that the asymptotic theory identifies at least three distinct lengthscales in $x$, namely

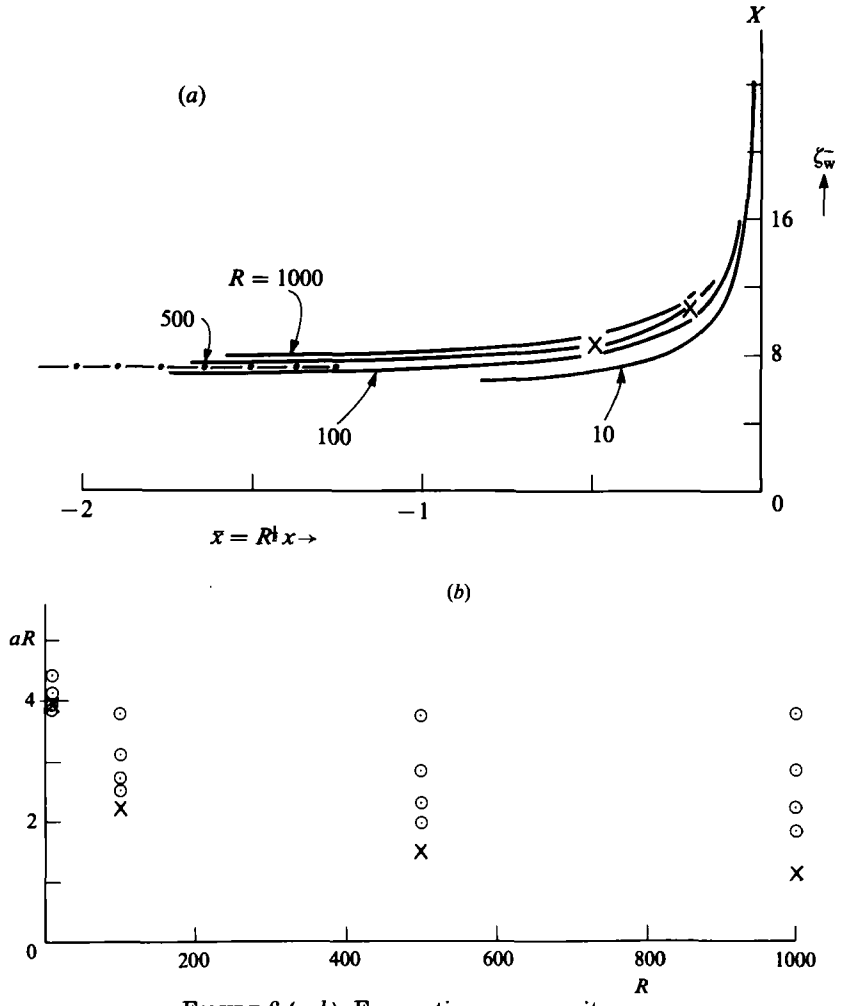


FIGURE 6 (*a–b*). For caption see opposite page.

$O(R)$, $O(R^{\frac{1}{7}})$ and $O(R^{-\frac{1}{2}})$; the lengthscale $x = O(1)$ also plays a significant role, albeit at higher order; and there are four scales involved in $y$, namely $O(1)$, $O(R^{-\frac{2}{7}})$, $1-O(R^{-\frac{2}{7}})$ and $O(R^{-\frac{1}{2}})$. Consequently, except at 'unambiguous' positions such as $(x, y) = (0, 0)$, $(0, 1)$ and $(\pm\infty, y)$, a little care has to be exercised in interpreting the asymptotic predictions appropriately. As it turns out, the numerical solutions themselves appear to single out the projected lengthscales satisfactorily for increasing $R$, as described below.

Figures 6(*a–d*) present quantitative comparisons between the numerical results described in §2, for finite values of $R$, and the asymptotic predictions described in §3. First, in figure 6(*a*) we plot the vorticity $\zeta_w^-$ on the splitter plate against $\bar{x} = R^{\frac{1}{2}}x$ just upstream of the trailing edge, to make comparisons with the local predictions noted in the penultimate paragraph of §3. The agreement is fairly good, both relatively far upstream (on the scale of figure 6*a*), where the value 7.22 of $\zeta_w^-$ from (3.31) is supposed theoretically to apply, and relatively close to the trailing edge, where the numerical results as $R$ increases are not inconsistent with the trend (3.34). In-between also comparison is quite favourable overall, although the results for $R = 500$ are slightly closer to the asymptotic predictions than are the results for

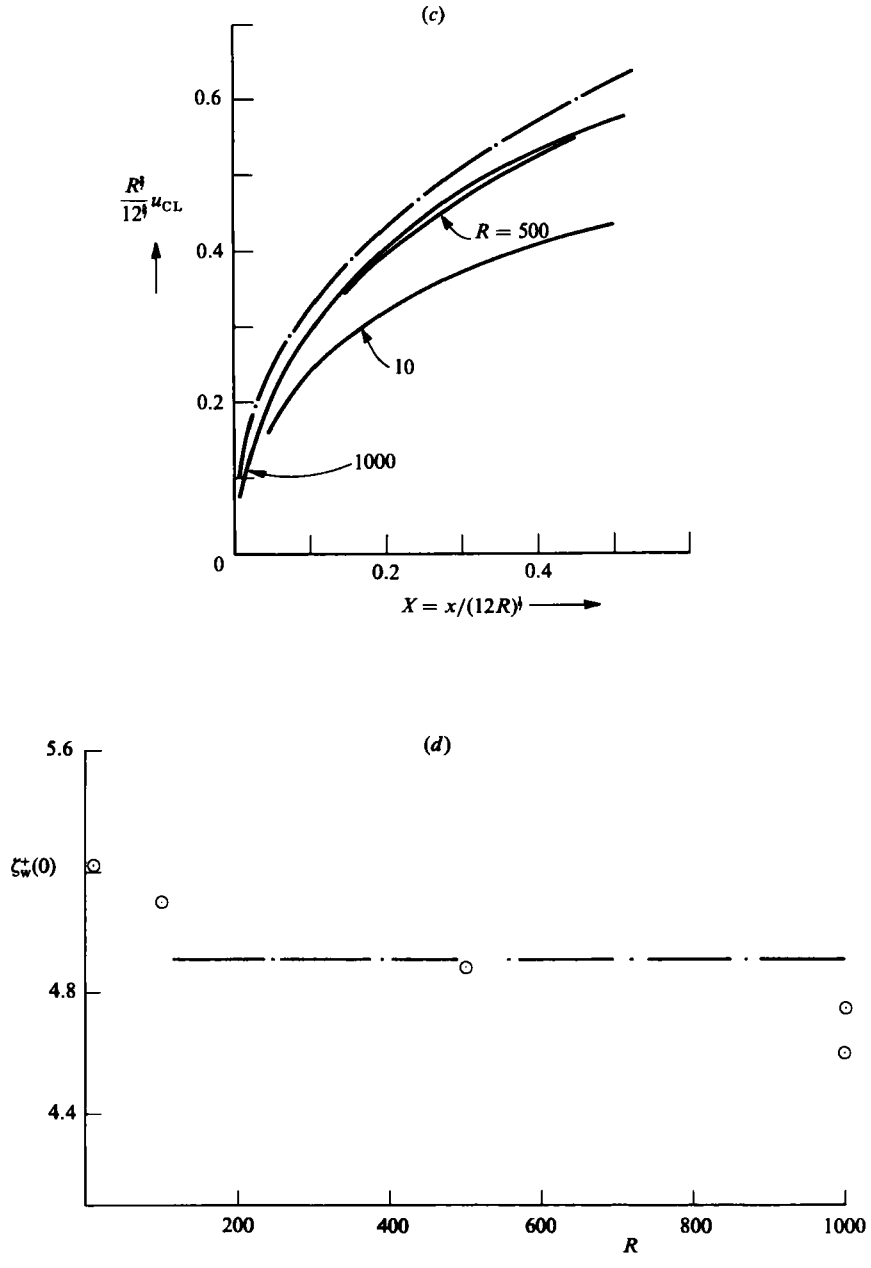


FIGURE 6. Comparisons between the numerical solutions described in §2 and the asymptotic theory described in §3, for increasing $R$. (*a*) Shear stress $\zeta_w^- \equiv \zeta(x,0)$ versus $\bar{x} \equiv R^{\frac{1}{2}}x < 0$ on the splitter plate: ——, numerical results from §2; ×, from §3 with Dijkstra (1974) (see penultimate paragraph of §3); –·–, upstream limit value from (3.31). (*b*) $aR$ versus $R$, where $a$ is the value of $-2\zeta_w^- |x|^{\frac{1}{2}} R^{-1}$ as $x \to 0-$ referred to in §2: ×, from the asymptotic prediction (3.34); ⊙, numerical results from §2 on four computational grids. Here each grid refinement *reduces* the value of $aR$ at each fixed $R$. (*c*) The reduced wake centreline velocity $R^{\frac{1}{2}}u_{CL}\,12^{-\frac{1}{4}}$ versus $X = (12R)^{-\frac{1}{4}}x$, where $u_{CL} \equiv u(x,0)$: ——, numerical results from §2; –·–, asymptote $U(X,0)$ from the solution of (3.4)–(3.7) and (3.9)–(3.14). (*d*) The shear stress $\zeta_w^+(0) \equiv \zeta(0,1)$ versus $R$: –·–, the asymptote $\tilde{\tau}(0)$ in (3.31); ⊙, numerical results from §2 on various computational grids; the grid refinement produces the upper value ⊙ at $R = 1000$.

$R = 1000$. Moreover, the comparisons indicate clearly that in a numerical sense the local behaviour (2.14) or (3.34) holds only at positions extremely close to the trailing edge, at the larger values of $R$; nevertheless, the calculations of §2 still tend to agree with (3.34) increasingly as the computational grid is refined even at such values of $R$. Another view of this aspect is given in figure 6(*b*), where both the influence of grid refinement at various Reynolds numbers $R$ and a comparison with the asymptote from (3.34) are presented for the coefficient $a(R) = \lim_{x\to 0-} (2\zeta_{\mathrm{w}}^{-} |x|^{\frac{1}{2}}/R)$. Increasing grid refinement tends to bring the calculations and the one-term asymptote much closer together.

Figure 6(*c*) compares the numerical and asymptotic solutions for the centreline velocity $u_{\mathrm{CL}}$ for $x > 0$, but plotted in the form $R^{\frac{2}{7}} u_{\mathrm{CL}} 12^{-\frac{5}{7}}$ versus $x(12R)^{-\frac{1}{7}}$ suggested by §3 as the universal limit form as $R\to\infty$. The closeness of the agreement here seems relatively encouraging for the $O(R^{\frac{1}{7}})$ scale theory, whereas the previous comparisons of figures 6(*a*, *b*) tend to emphasize the practical importance of the $O(R^{-\frac{1}{2}})$ subscale just upstream instead. That subscale is responsible for a small shift of origin, which could be applied if necessary to extend the one-term limiting prediction in figure 6(*c*) into a two-term expansion, but that shift is not included here. Also it is worth noting the presence of the still longer-scale zone $x = O(R)$ further downstream in which the limit curve of figure 6(*c*) again becomes invalid. Finally, figure 6(*d*) presents a comparison between the numerical and asymptotic results for the shear stress $\zeta_{\mathrm{w}}^{+}(0)$ on the outer wall at the station $x = 0$. A further comparison concerning the variation of $\zeta_{\mathrm{w}}^{+}$ with $x$, as $R$ increases, is not possible here since the asymptotic properties of the difference $\zeta_{\mathrm{w}}^{+} - \zeta_{\mathrm{w}}^{+}(0)$ on the $O(1)$ scale in $x$ around $x = 0$ are not yet known, but the agreement concerning the value of $\zeta_{\mathrm{w}}^{+}(0)$ in figure 6(*d*) is quite good over a wide range of values of $R$, apart from the remaining possibly grid-dependent undershoot at $R = 1000$.

If we bear in mind the inevitable difficulties, however major or minor, regarding the interpretation of lengthscales on the analytical side and the distribution of the computational grid on the numerical side, we feel that although the measure of agreement is not absolutely conclusive it does favour belief in the value of both the analytical and numerical work. On the numerical side the techniques described in §2 for the treatment of the discontinuity at the trailing edge and of the flow conditions far upstream and downstream seem to prove satisfactorily accurate in most respects. The third main difficulty, that of obtaining convergence of the iterative scheme at the larger values of $R$, is handled adequately as before (Dennis & Hudson 1978) by the extended differencing outlined in §2. The asymptotic approach likewise draws some encouragement from the comparisons above. Apart from the support for the correctness of the limiting account in §3 as $R\to\infty$, it is an interesting sign also that the results of the asymptotic theory prove useful at moderate† values of $R$, even though terms as slowly varying as $R^{\frac{1}{7}}$ are involved.

Applications of both the computational and the asymptotic techniques to other, perhaps more complicated, internal flows concerning branchings or similar basic disturbances would seem well worth while. The effects of non-symmetry, cornering, curving and constriction as well as branching are of considerable practical and theoretical interest, whether in planar channel flows or three-dimensional pipe flows.

The financial support of the Natural Sciences and Engineering Research Council of Canada, for F.T.S. during 1978–79, and of the Science Research Council, U.K.,

† Note for comparison that the critical Reynolds number below which the motion remains linearly stable is $R \approx 7700$ in the Poiseuille flow far upstream, and $R \approx 3850$ far downstream.

for S. B. during 1975–78, are gratefully acknowledged. The computations of solutions of the Navier–Stokes equations were also supported by the Natural Sciences and Engineering Research Council of Canada. Thanks are due to the referees for helpful comments.

## REFERENCES

BATES, S. 1978 Ph.D. thesis, University of London.

BRAMLEY, J. S. & DENNIS, S. C. R. 1982*a* The calculation of eigenvalues for the stationary perturbation of Poiseuille flow. *J. Comp. Phys.* **47**, 179.

BRAMLEY, J. S. & DENNIS, S. C. R. 1982*b* A numerical treatment of two-dimensional flow in a branching channel. In Lecture Notes in Physics vol. 170, p. 155. Springer.

BRAMLEY, J. S. & DENNIS, S. C. R. 1984 The numerical solution of two-dimensional flow in a branching channel. *Comp. Fluids* (to appear).

DANIELS, P. G. 1974 Numerical and asymptotic solutions for the supersonic flow near the trailing edge of a flat plate. *Q. J. Mech. Appl. Maths* **27**, 175.

DENNIS, S. C. R. & HUDSON, J. D. 1978 A difference method for solving the Navier–Stokes equations. In *Numerical Methods in Laminar and Turbulent Flow*, p. 69. Pentech.

DENNIS, S. C. R. & SMITH, F. T. 1980 Steady flow in a channel with a symmetrical constriction in the form of a step. *Proc. R. Soc. Lond.* A **372**, 392.

DIJKSTRA, D. 1974 Ph.D. thesis, University of Groningen.

GOLDSTEIN, S. 1930 Concerning some solutions of the boundary-layer equations in hydrodynamics. *Proc. Camb. Phil. Soc.* **26**, 1.

HAKKINEN, R. J. & ROTT, N. 1965 Similar solutions for merging shear flows. *AIAA J.* **3**, 1553.

PEDLEY, T. J. 1980 *The Fluid Mechanics of Large Blood Vessels.* Cambridge University Press.

SMITH, F. T. 1976 Flow through constricted or dilated pipes and channels, Part 2. *Q. J. Mech. Appl. Maths* **29**, 365.

SMITH, F. T. 1977*a* Steady motion through a branching tube. *Proc. R. Soc. Lond.* A **355**, 167.

SMITH, F. T. 1977*b* Upstream interactions in channel flows. *J. Fluid Mech.* **79**, 631.

SMITH, F. T. 1978 A note on a wall jet negotiating a trailing edge. *Q. J. Mech. Appl. Maths* **31**, 473.

SMITH, F. T. & DENNIS, S. C. R. 1981 Injection from a finite section of a flat plate placed parallel to a uniform stream. *J. Engng Maths* **15**, 267.

SMITH, F. T. & DUCK, P. W. 1980 On the severe nonsymmetric constriction, curving or cornering of channel flows. *J. Fluid Mech.* **98**, 727.

SMITH, F. T. & STEWARTSON, K. 1973 On slot-injection into a supersonic laminar boundary layer. *Proc. R. Soc. Lond.* A **322**, 1.

STEWARTSON, K. 1970 On supersonic laminar boundary layers near convex corners. *Proc. R. Soc. Lond.* A **319**, 289.

VAN DYKE, M. 1970 Entry flow in a channel. *J. Fluid Mech.* **44**, 813.

WILSON, S. 1971 Entry flow in a channel. Part 2. *J. Fluid Mech.* **46**, 787.

WOODS, L. C. 1954 A note on the numerical solution of fourth order differential equations. *Aero. Q.* **5**, 176.